International Journal of Thermodynamics (IJoT)
ISSN 1301-9724 / e-ISSN 2146-1511
https://dergipark.org.tr/en/pub/ijot

Vol. 28 (No. 1), pp. 007-016, 2025
doi: 10.5541/ijot.1517744
Published online: March 1, 2025

Research Article

Exact Thermodynamic Solution of Gas Behavior in Propellant Tanks and Storage Capsules During Pressurization

*M. Mohseni

Department of Mechanical Engineering, Qom University of Technology, Qom 37181 46645, Iran
E-mail: *m.mohseni@qut.ac.ir

Received 20 July 2024, Revised 15 September 2024, Accepted 15 November 2024

Abstract

The gas properties, particularly the pressure within the propellant tanks of a liquid-fueled rocket, play an essential role in the performance of the propulsion system. This study examines the thermodynamic behavior of the gas inside the propellant tanks and gas storage capsules of a class of pressurized systems. To this end, the governing thermodynamic equations were extracted, and exact thermodynamic solutions for the changes in the gas properties were obtained. The changes in the gas properties have been studied during the whole operation of the propulsion system, i.e. in the pre-pressurization period and before and after the gas cut-off time. A comparison of the analytical modelling results with the experimental data indicates a good agreement between the two, with the total mass of gas required for tank pressurization being approximately 4% higher than the experimental data. Additionally, the approximate changes in the throat area of the pressure-reducing valve were obtained. The simple thermodynamic model developed in this study allows for the rapid design and observation of the pressurization system's performance.

Keywords: *Propulsion system; pressurization system; thermodynamic modeling; analytical solution, rapid design.*

1. Introduction

The transient flow of two phases of gas and liquid in a tank is present in many cases, including the propellant tanks of a liquid fuel rocket [1], [2]. Liquid rockets require a pressurization system to pressurize the fuel and oxidizer in order to transfer them to the propellant pumps at the required flow and pressure [3]. The gas is placed in the upper space of the tanks, which is called ullage [2], [3]. The gas properties within the ullage, particularly the pressure, have been demonstrated to exert a substantial influence on the system's performance. This assertion has been the subject of extensive research, the findings of which are discussed in the following section.

In et al. [3] studied a liquid helium pressurization system that utilized an electrical heater to improve the performance of the system with thermodynamic and experimental methods. Majumdar et al. [4] developed a numerical model of self-pressurization of a cryogenic tank in ground operation using GFSSP code. In their model, the effect of liquid phase evaporation is considered in a relatively simple way. Zilliac [5] developed a thermodynamic model for changing the properties of gas in a pressurization system which models the self-pressurizing oxidizer system of a moderate-size hybrid rocket. In his model, the effect of mass and heat transfer between the two phases as well as heat transfer between the gas and the tank wall is considered. Karimi et al. [6] developed a thermodynamic model for a neutral gas storage type pressurization system in a liquid fuel rocket. Comparison with experimental data shows that the performance of their model is satisfactory. Using thermo-fluid relationships, Gieras, and Gorgeri [7] developed a mathematical model for the discharge of gas and liquid in the propulsion tank and the combustion rate of fuel in a hybrid liquid-solid rocket engine. Their model was calibrated using experimental results and could be used for preliminary design. Wang et al. [8] investigated the pressurization process in a liquid hydrogen tank during discharge using the Fluent 6.3 CFD code. They examined the effect of phase change and the structure of the injector (direction of gas to enter the tank). According to their results, phase change has little influence on the behavior of the system so it can be ignored for convenience in numerical simulation. In another study, Wang et al. [9] investigated the effects of inlet temperature, injector structure, ramp time, wall thickness, and outflow rate on the performance of a pressurization system in a cryogenic tank. They showed that the effect of gas inlet temperature, and injector structure are high. Zuo et al. [10] numerically examined the flow of two liquid-vapor phases into a cryogenic tank of self-pressurization. They used Open Foam as a programming environment. According to their results, the speed of calculations of this program is several times faster than conventional software.

Given the numerous advantages of hydrogen (H_2), including high energy density, cleanliness, and carbon neutrality, Ali et al. [11] conducted an investigation into the potential opportunities for H_2 storage technologies, including physical and chemical storage, as well as the recent developments and challenges regarding hydrogen storage. The insulation of fuel storage tanks represents a significant topic of investigation, as evidenced by the work of Yin et al. [12]. A review of the recent progress in passive thermal protection technologies employed in the insulation structure of LH_2 storage tanks was conducted. One method of insulation or controllable release of energy is the application

*Corresponding Author

of a coating to the storage tank, as demonstrated by Fan et al. [13]. The impact of fluidized bed coating temperature, air velocity, flow speed, and atomization pressure on the adhesion rate, coating integrity, and coating uniformity of the coated spherical propellant was examined in the study. Wang et al. [14] established a CFD model to investigate the wall insulation of a cryogenic tank during discharge on the pressurization system. Their results show that the inner insulation layer can significantly reduce the gas requirement which is more significant with the increase of inlet gas temperature. Li et al. [15] numerically examined the operating process in the spherical tank of a hydrogen liquid rocket. They performed their solution in two dimensions using the ANSYS Fluent 17 commercial software. This software is utilized extensively for the analysis of fluid mechanics issues, encompassing a multitude of physical phenomena, including multiphase and turbulent flows. In the study of Li et al. [15], the VOF model is used to solve the two-phase flow and the RNG k-ε to model the turbulent flow. According to their results, fluid phase change leads to an increase in the amplitude of temperature fluctuations. In another study, Li and Liang [16] simulated the mass and heat transfer between the two phases of gas and liquid inside the hydrogen tank during the pressurization process. They investigated the effect of temperature and mass flow rate of the inlet gas as well as its direction of spraying on the problem. In the work of Wang et al. [17], in addition to heat transfer inside the tank, the effect of aerodynamic heating is also considered. Based on their results, in ordinary conditions outside aerodynamic heating cannot penetrate the foam layer to facilitate the pressurization performance. In other words, if the thermal performance of the outer surface of the tank wall does not have a specific case, the effect of aerodynamic heating in the CFD simulation of a foam-insulated tank can be ignored. Mitikov and Shynkarenko [18] suggested a method to reduce the final mass of the pressurization system by two commands from the control system to open the drain valve and close it. In this regard, energy management equipment can be employed to enhance system performance and reduce its weight, as demonstrated by Yilmaz et al. [19]. Barsi, and Kassemi [20] developed a two-phase lumped vapor CFD model which was used to describe the self-pressurization behavior of a tank partially filled with LH_2 in normal gravity. Their model is somewhat consistent with the experimental data. Numerical results of Panzarella, and Kassemi [21] which investigated the pressurization of a large cryogenic storage tank indicate that in microgravity both buoyancy and natural convection are still important and play a significant role in phase distribution and tank pressurization. Fester and Bingham [22] studied numerous propellant combinations to form a small combustion zone. The resulting hot combustion gases were used to pressurize the tank to operating pressure and then maintain this pressure during outflow. One method for enhancing the efficiency of combustion energy release is to optimize the detonation process, which is the focus of Yang's [23] research. In light of these findings, it may be posited that high-performance heritage solid fuels for pyrotechnics, such as boron, titanium hydride, and carbon, could be employed as injectants for the enhancement of detonation performance, thereby mitigating the effects of transients in high-pressure, high-rate gaseous injection, as exemplified by scramjets. In a recent publication, Scholl et al. [24] presented a novel concept of microencapsulated hydrocarbon fuels for the development of a monopropellant system. This system is employed in rocket engines when the requisite reliability and technical simplicity are paramount.

While the research conducted thus far has yielded valuable insights, it is imperative to continue investigating this field to gain a more comprehensive understanding. Previous studies have typically employed the use of commercial software for the detailed examination of flow patterns. Other researchers have developed a thermodynamic model that necessitates a numerical solution. Moreover, the majority of existing research has focused on self-pressurization systems, with comparatively limited investigation of pressurization systems for gas storage. Accordingly, the present study employs a straightforward analytical thermodynamic model to examine the functionality of a pump-fed gas storage pressurization system in a liquid fuel rocket. To this end, the behavior of the gas within the propellant tanks and the gas storage capsules has been examined, and the quantity of gas necessary for each tank has been determined.

2. Problem Description

Figure 1 depicts a schematic representation of the pump-fed gas storage type pressurization system in a liquid rocket.

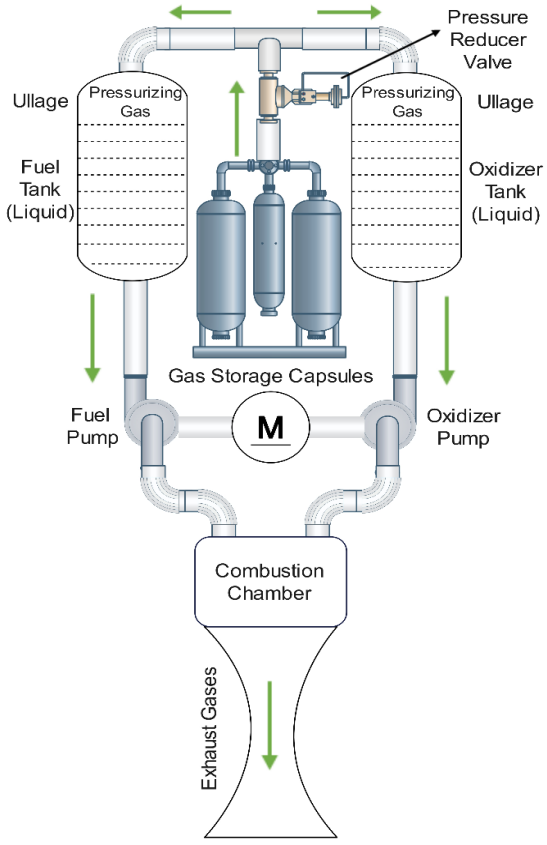

Figure 1. Schematic of the gas-storage pressurization system.

The operation of this system is as follows: the pressurizing gas, after flowing from its storage capsules in which it is kept under high pressure, passes through a pressure-reducing valve and then enters the fuel and oxidizer tanks, where it exerts pressure on them. This pressure is essential for the prevention of cavitation in engine pumps during operation. It is crucial to acknowledge that the storage of gas at high pressure in capsules serves the purpose of reducing the overall volume and mass of the system. The gas is utilized in a gradual manner throughout the course of the flight.

In liquid fuel rockets, the gas typically flows around the engine in order to gain heat before entering the tanks, thereby elevating its temperature and, consequently, its pressure. This process results in a reduction in the quantity of gas required for pressurization and cooling of the engine wall, although it introduces additional complexity into the system.

As illustrated in Figure 1, the upper portion of the tank depicts the volume of the pressurizing gas. As previously stated, the term "ullage" is used to describe the space above the liquid fuel or oxidizer within the tanks into which the gas is introduced. The selection of the pressurizing gas is also a significant factor, with implications for the overall mass of the rocket. This indicates that gases with a lower molar mass than air, such as helium, can be an effective means of reducing the mass of the system, provided that the system is adequately sealed. For a more thorough examination of the system's functionality, readers are directed to consult reference [25].

3. Thermodynamic Modeling

The first law of thermodynamics for a control volume in the transient state is as follows [26].

$$\dot{Q} - \dot{W} + \sum \dot{m}_i \theta_i - \sum \dot{m}_e \theta_e = \frac{dE}{dt} \tag{1}$$

where

$$\theta = h + \frac{V^2}{2} + gz \tag{2}$$

is the energy of a flowing fluid and

$$\Delta E = \Delta U + \Delta Ke + \Delta Pe \tag{3}$$

is the change of system energy. In Eq. (1), $\dot{Q}$ *and* $\dot{W}$ are the rate of heat transfer and rate of work, respectively. Aditionally, *h, V, z, U, Ke*, and *Pe* represent enthalpy, velocity, elevation, internal energy, kinetic energy and potential energy.

By ignoring the changes in kinetic and potential energies of the system as well as the heat transfer term Eq. (1) can be simplified as follows.

$$-\dot{W} + \sum \dot{m}_i h_i - \sum \dot{m}_e h_e = \frac{dU}{dt} \tag{4}$$

It should be noted that although changes in kinetic and potential energies alone can be significant, they are negligible in comparison to changes in enthalpy. Additionally, while heat transfer does influence the outcomes to a degree, its intricate mechanism which encompasses both natural and forced convection, as well as the aerodynamic heating of the flying device's outer wall makes it challenging to model with precision.

As mentioned before, two important elements of the pressurization system are the gas storage capsules and the propellant tanks which their equations discuss separately in the two following sections.

3.1 Propellant Tanks

Considering the ullage as the control volume and with one input to the ullage, Eq. (4) becomes as follows.

$$\frac{dU}{dt} = \dot{m}_i h_i - p\dot{V} \tag{5}$$

In the above equation, p is gas pressure inside the tank, $\dot{m}_i$ is the mass flow rate of the gas entering the tank, and $\dot{V}$ is the gas volume expansion rate. Considering the temperature and pressure range in the tank, the ideal gas equation of state can be used. Under these conditions, the internal energy of the gas is obtained from the following relation.

$$U = mC_v T = \frac{PV}{k-1} \tag{6}$$

By differentiating the above relation with respect to time and combining the result with Eq. (5), the following equation is obtained for changes in gas pressure inside the tank.

$$\frac{dp}{dt} = \frac{k-1}{V(t)} \dot{m}_i h_i - \frac{kp}{V(t)} \frac{dV}{dt} \tag{7}$$

In deriving Eq. (7), the following assumptions have been made.

1- $k = C_p/C_v$ has a constant value in which C_p and C_v are gas specific heats.
2- The different properties of the gas inside the ullage are homogeneous and uniform. In other words, they change only with time.
3- The mass transfer between liquid and gas phases due to evaporation and condensation is neglected. It should be noted that in the pressurization system of the neutral gas storage type, unlike the self-pressurization type, this assumption is reasonable.
4- Heat transfer between gas and its environment has been neglected.

In addition to the numerical solution, for the conditions of the present study, Eq. (7) has an analytical solution. To do this, Eq. (7) can be written as Eq. (8).

$$\frac{dP}{dt} + f(t)P = g(t) \tag{8}$$

where,

$$f(t) = k \frac{\dot{V}}{V(t)} \tag{9}$$

and

$$g(t) = \frac{k-1}{V(t)} \dot{m}_i h_i \tag{10}$$

For an ideal gas, Eq. (10) may be written as Eq. (11).

$$g(t) = \frac{k-1}{V(t)} \dot{m}_i c_p T_i \tag{11}$$

Equation (8) is a first-order linear ordinary differential equation with the following answer [27].

$$p(t) = \frac{1}{\lambda} \int g(t) \lambda dt + \frac{p_0}{\lambda} \tag{12}$$

where,

$$\lambda = e^{\int f(t) dt} \tag{13}$$

During the entire engine operation time, the mass flow rate of the liquid from the tanks is constant. As a result, the volume of the gas in the tank will be a linear function of time, which is obtained from the following equation.

$$V(t) = V_0 + \dot{V}t \tag{14}$$

In Eq. (14) V_0 is initial volume of the gas. Also in this study, based on experimental results [6] and for modeling convenience, the mass flow rate of the inlet gas is considered a constant or a linear function of time depending on the period of the pressurization process. For these conditions, it can be written as:

$$\dot{m}_i = a + bt \tag{15}$$

where a and b are constant.

Using the equations above, we can find the answer to Eq. (8). This answer shows the changes in gas pressure inside the tank during engine operation.

$$p(t) = \frac{RT_i}{\dot{V}V(t)^k}\left\{\dot{m}_i(t)V(t)^k - \dot{m}_{i0}V_0^k - \frac{b}{(k+1)\dot{V}}[\mathrm{V}(t)^{k+1} - V_0^{k+1}]\right\} + p_0\left[\frac{V_0}{V(t)}\right]^k \tag{16}$$

In the above equation, R is the gas constant, and p_0 is the initial pressure of the gas. In general, the answer to Eq. (8) is obtained by numerical calculation methods such as Euler or Range-Kutta [28].

The density of the gas inside the tank is also obtained from the following equation.

$$\rho(t) = \frac{m(t)}{V(t)} = \frac{1}{V(t)}\left(m_0 + \int \dot{m}_i\, dt\right) \tag{17}$$

where m_0 is the initial mass of the gas inside the tank. To obtain the temperature at any instant in time, the ideal gas equation of state can be used as follows.

$$T(t) = \frac{p(t)}{\rho(t)R} \tag{18}$$

3.2 Gas Storage Capsules

For gas-storage capsules with no work, Eq. (4) becomes as follows.

$$-\dot{m}_e\left(h_e + \frac{V_e^2}{2}\right) = \frac{dU}{dt} \tag{19}$$

Using the ideal gas equation and the definition of internal energy, i.e. Eq. (4), Eq. (19) can be written as

$$-\dot{m}_e\left(C_pT_e + \frac{V_e^2}{2}\right) = C_v m\frac{dT}{dt} + C_vT\frac{dm}{dt} \tag{20}$$

Due to the large difference between the gas pressure inside the capsules and the outlet pressure of the reducer valve, flow chokes at the outlet of the valve, and the Mach number becomes equal to 1 [29]. This means that the speed of the gas is equal to the speed of sound. As a result, we will have:

$$-\dot{m}_e\left(\frac{kR}{k-1}T_e + \frac{kRT_e}{2}\right) = C_v m\frac{dT}{dt} - C_vT\dot{m}_e \tag{21}$$

By simplifying the above equation and the relationship between the outlet static temperature and the stagnation temperature inside the capsule, we can write [29]:

$$(1-k)\dot{m}_eT = m\frac{dT}{dt} \tag{22}$$

In the case of chocked flow, the mass flow rate of the gas is obtained from the following relation [29].

$$\dot{m} = fA^*\frac{p}{\sqrt{T}} \tag{23}$$

where,

$$f = \sqrt{\frac{k}{R}\left(\frac{2}{k+1}\right)^{\frac{k+1}{k-1}}} \tag{24}$$

Here A^* is the area of the critical throat where the Mach number is equal to 1. Thus, Eq. (22) can be written as

$$(1-k)fA^*\frac{\rho RT}{\sqrt{T}}T = \rho\forall\frac{dT}{dt} \tag{25}$$

or

$$-\frac{(k-1)}{\forall}fA^*RT^{3/2} = \frac{dT}{dt} \tag{26}$$

By solving the above equation and a little algebraic operation, the temperature changes of the gas inside the capsule will be as follows.

$$T = \frac{T_0}{\left\{\left[\frac{(k-1)}{2\forall}fA^*R\sqrt{T_0}\right]t+1\right\}^2} \tag{27}$$

where T_0 is the initial temperature of the gas and $\forall$ is the capsule volume. The Eq. (27) can be written as a simple form as Eq. (28).

$$\frac{T}{T_0} = (1+Bt)^{-2} \tag{28}$$

where,

$$B = \left[\frac{(k-1)}{2\forall}fA^*R\sqrt{T_0}\right] \tag{29}$$

The changes in gas density are equal to

$$\frac{d\rho}{dt} = -\frac{\dot{m}}{\forall} \tag{30}$$

Using the mass flow rate formula and the ideal gas equation, we will have

$$\frac{d\rho}{\rho} = -\frac{fA^*R}{\forall}\frac{T}{\sqrt{T}}dt \tag{31}$$

which can be written as Eq. (32) by applying the temperature equation.

$$\frac{d\rho}{\rho} = -\frac{fA^*R\sqrt{T_0}}{\forall}\frac{dt}{(1+Bt)} \tag{32}$$

By solving the above equation, the gas density changes inside the capsule are obtained as follows.

$$\frac{\rho}{\rho_0} = (1+Bt)^{-\frac{2}{k-1}} \tag{33}$$

where B is defined in Eq. (29). By applying the ideal gas equation, the gas pressure variations are obtained as Eq. (34).

$$\frac{p}{p_0} = (1 + Bt)^{-\frac{2k}{k-1}} \quad (34)$$

By knowing the amount of mass of the gas required for pressurization, the number of gas storage capsules can be obtained. In this instance, the following relationship exists between the pressure, temperature, volume, mass, and number of gas storage capsules (N), whereby Z represents the gas compressibility factor.

$$p(N\forall) = mZRT \quad (35)$$

It is important to note that $\forall$ represents the volume of each individual capsule. Therefore, $N\forall$ represents the total volume of all capsules. For calculating the compressibility factor, the famous Lee-Kesler equation of state can be used [30].

$$Z = \frac{P_r v_r}{T_r} = 1 + \frac{B}{v_r} + \frac{C}{v_r^2} + \frac{D}{v_r^5} + \frac{c_4}{T_r^3 v_r^2}\left(\beta + \frac{\gamma}{v_r^2}\right) exp\left(-\frac{\gamma}{v_r^2}\right) \quad (36)$$

in which

$$B = b_1 - \frac{b_2}{T_r} - \frac{b_3}{T_r^2} - \frac{b_4}{T_r^3} \quad (37)$$

$$C = c_1 - \frac{c_2}{T_r} + \frac{c_3}{T_r^3} \quad (38)$$

$$D = d_1 + \frac{d_2}{T_r} \quad (39)$$

and

$$T_r = \frac{T}{T_{cr}}, P_r = \frac{p}{P_{cr}}, v_r = \frac{vP_{cr}}{RT_{cr}} \quad (40)$$

where T_{cr}= *132.5 K*, P_{cr}= *37.7 bar*, and ρ_{cr}= *11.325 kg/m*^{3} are the critical temperature, critical pressure, and critical density of the gas, respectively. Also, the constants utilized in the aforementioned equation can be found in Ref. [30].

4. Results and Discussion

In this section, the performance of the obtained thermodynamic model is evaluated by comparing its results with experimental data [6]. The conditions utilized for the calculation of the results, as well as the properties of the liquids and the gas, are presented in Tables 1 and 2.

Table 1. Liquid properties and solution conditions.

Quantity	Upper tank	Lower tank
Density	804 kg/m^3	1596 kg/m^3
Mass flow rate	25 kg/s	92 kg/s
Initial temperature	300 K	300 K
Initial pressure	1.4 bar	0.86 bar
Required ullage pressure	6 bar	6.2 bar

Table 2. Gas properties and solution conditions.

Quantity	Upper tank	Lower tank
Density	Ideal gas	Ideal gas
Specific heat capacity	1005 J/kg.K	1005 J/kg.K
Initial volume	0.19 m^3	0.3 m^3
Inlet temperature	425 K	425 K
Initial temperature	300 K	300 K
Relative cut-off time	0.29	----

In accordance with the aforementioned conditions, the variations in gas pressure within the ullage of the lower and upper tanks are illustrated in Figures 2 and 3. The relative time represented in these figures is obtained by dividing the instantaneous time by the total time of engine operation.

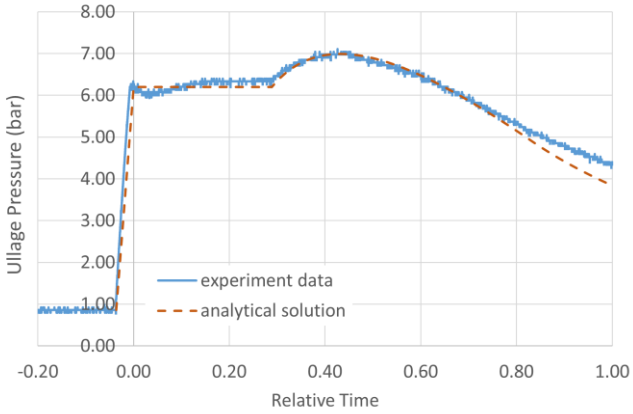

Figure 2. Comparison of changes in gas pressure inside the lower tank obtained from the thermodynamic model with experimental data [6].

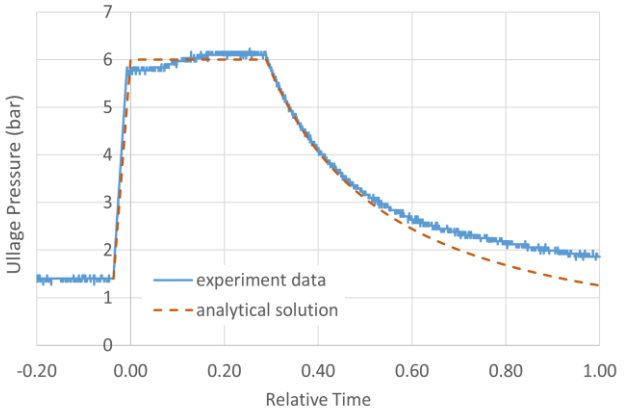

Figure 3. Comparison of changes in gas pressure inside the upper tank obtained from the thermodynamic model with experimental data [6].

According to these figures, the total operating time of the pressurization system is divided into three parts. The first section of the figures is the pre-pressurization period until the tank pressure reaches the nominal value of about 6 bar and then the engine starts. The second stage is from the time the engine is started until the gas is cut to the upper tank. And the third part is from the time of cutting the gas to the end of the engine operation. It should be noted that the reason for cutting off the inlet gas to the upper tank is to provide the required ullage pressure by the amount of gas entering the tank up to this point and the effect of acceleration of the rocket. As a result, to reduce the mass of the gas, its inlet to the upper tank is cut off after a while. In these situations, the efficacy of sensors and the reliability of a robust model for their estimation can have a significant impact on the management of rocket engine health [31].

It is observed from Figures 2 and 3 that after shutting off the inlet gas to the upper tank its pressure decreases while for the lower tank, on the contrary, its pressure increases. This is because after cutting off the gas in the upper tank, the total mass flow of the gas enters the lower tank. Also, as can be seen, except for the final moments of the engine operation,

where the difference between the modeling results and the experimental data for the upper tank is significant, in other cases, there is a good agreement between the two. The reason for this difference is the heat transfer from the tank walls, which is affected by aerodynamic heating, to the internal gas, which has been neglected in thermodynamic modeling. More explanation is that a reduction in gas pressure within the upper tank at the end time of the system's operation, as illustrated in Fig. 3, results in a decline in gas temperature, reaching a point below that of the tank wall temperature. This phenomenon initiates a heat transfer from the wall, which has been subjected to aerodynamic heating and is consequently at a higher temperature, to the gas, leading to an increase in its temperature and pressure. According to Figure 3, this difference increases as the engine runs out of time when the pressure and consequently the upper tank temperature are significantly reduced. Given that the modeling results predict the pressure to be less than the actual value, this can be considered a reliability factor for designing the pump inlet pressure.

To see the gas temperature changes, diagrams for both the upper and lower tanks are plotted in Figure 4. As can be seen, the gas temperature of the upper tank drops to about 260 K (-13 °C) due to the cut-off of the inlet gas.

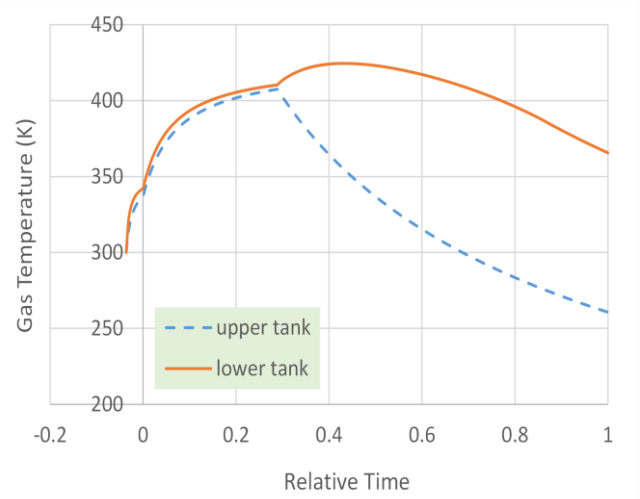

Figure 4. Changes in gas temperature inside the propellant tanks using the present model.

Using Eq. (7), the required mass flow rate of the gas in the pre-pressurization process can be calculated from the following equation.

$$\dot{m}_{i1} = \frac{(p-p_0)V_0}{kR\,T_i t_1} \tag{41}$$

where t_1 is the pre-pressurization time and p is the pressure required at the end of the pre-pressurization time to start the engine. Also, the mass flow rate of the gas in the second stage, when the gas pressure remains almost constant, is obtained approximately from the following equation.

$$\dot{m}_{i2} = \frac{P}{R\,T_i} \cdot \frac{\dot{m}_l}{\rho_l} \tag{42}$$

where $\dot{m}_l$ and ρ_l are the output mass flow rate of the liquid propellant and its density, respectively. In a real problem, the liquid fuel discharge from the tank is obtained based on the needs of the engine. Also, the inlet gas flow rate to the tank is determined based on the need for inlet pressure to the pumps. This pressure can be calculated from the following equation [6].

$$P_p = P_u + \rho H a - 0.58\rho V_p^2 - \rho h_L \tag{43}$$

where,

$$a = g\sin\theta + \ddot{x} \tag{44}$$

is the acceleration of the flying device and

$$H = H_0 - \frac{\dot{m}_l}{\rho_l A_t} t \tag{45}$$

is the height of the fluid from the level of the liquid propellant in the tanks to the pump inlet. In addition, V_p is the liquid velocity at the pump inlet and ρh_L is the pressure loss in the pipeline before the pump. It should be noted that the mass flow rate obtained from the Eq. (42) is the required mass flow rate or is an average value while it decreases almost linearly in the pre-pressurization period as follows.

$$\dot{m}_i = a + bt \tag{46}$$

Since the pre-pressurization time is before the zero time, so at the time $t=0$, $\dot{m}_i = \dot{m}_{i2}$. Thus, the constant 'a' will equal to $\dot{m}_{i2}$. To obtain the constant 'b' in Eq. (46), the Eq. (7) can be written as

$$\frac{dp}{dt} = \frac{k-1}{V_0}\dot{m}_i C_p T_i \tag{47}$$

By integrating the above equation and using Eqs. (42), (43), and (44), the value of 'b' is obtained as

$$b = 2\frac{(\dot{m}_{i1}-\dot{m}_{i2})}{t_1} \tag{48}$$

And thus, the relation for pre-pressurization mass flow rate can be written as the following equation.

$$\dot{m}_i = \dot{m}_{i2} + 2\frac{\dot{m}_{i1}-\dot{m}_{i2}}{t_1} t \tag{49}$$

According to previous discussions, changes in the mass flow rate of the inlet gas to the upper and lower tanks are shown in Figures 5 and 6 and compared with the experimental data. Such changes in mass flow rate occur in the type of liquid fuel rocket whose pressurization system uses gas storage capsules.

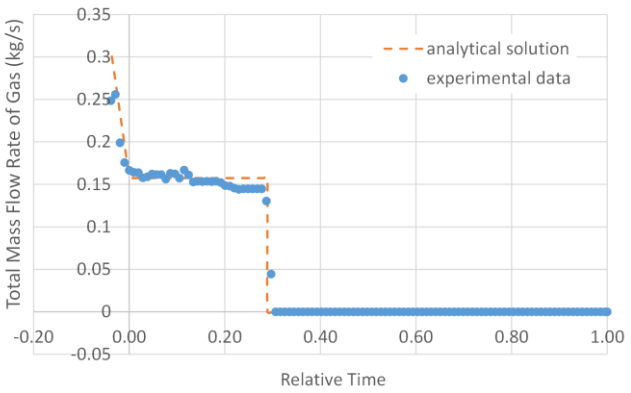

Figure 5. Changes in the mass flow rate of the inlet gas to the upper tank [6].

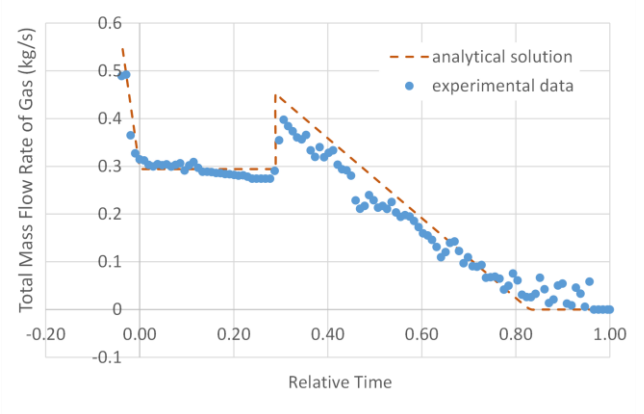

Figure 6. Changes in the mass flow rate of the inlet gas to the lower tank [6].

As mentioned earlier, the pre-zero time section is for the pre-pressurization period until the tank pressure reaches the nominal value and then the engine starts. The mass flow is then reduced to an almost constant value so that the tank pressure is maintained at its nominal value. It is observed that after cutting off the gas of the upper tank, the total mass flow rate enters the lower tank, and its flow rate increases at once.

Figure 7 shows the changes in the total mass flow rate to the tanks based on modeling results and experimental data. The values of this figure are equal to the sum of the values of the two Figures 5 and 6, which come out of the gas storage capsules and pass through the pressure-reducing valve.

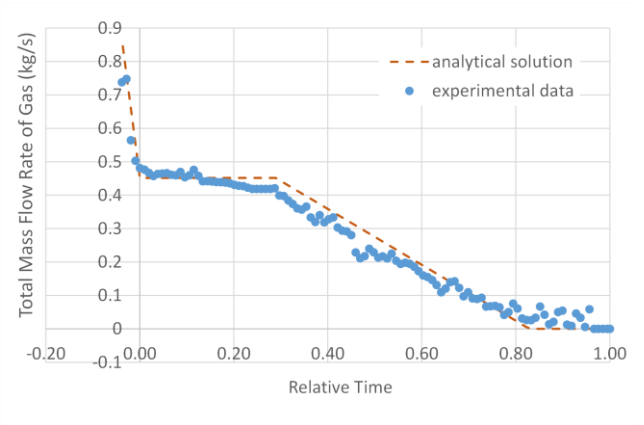

Figure 7. Changes in the total mass flow rate of the gas entering the tanks [6].

By integrating the above diagrams with respect to time, the mass of the consumed gas as a function of time is obtained which is shown in Figure 8. As can be seen, the difference in the final mass of the gas for the two diagrams is about 4%. By knowing the amount of mass of the gas required for pressurization, the number of gas storage capsules can be obtained.

Depending on the amount of mass consumed and the volume of the ullage at any given time, changes in gas density can be obtained during engine operation. The results so obtained for the gas density variations are plotted in Figures 9 and 10 for both lower and upper tanks. In this case, the maximum difference that occurs for the lower tank is less than 8 %. Generally speaking, there is a good agreement between the results of thermodynamic modeling and the experimental data. Table 3 shows the maximum difference for the various quantities including mass, pressure, and density of the gas for both upper and lower tanks during the whole time of engine operation.

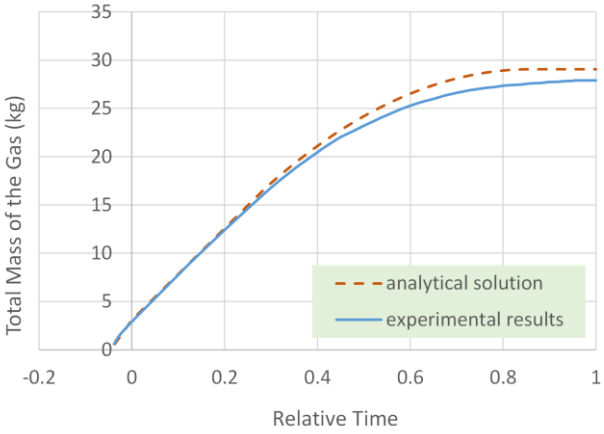

Figure 8. Changes in the total mass of the incoming gas to the tanks.

In the following, based on the relationships derived in Sec. 3.2, the time variations of the pressure and temperature of the gas inside the gas storage capsules are plotted in Figures 11 and 12 and compared with the experimental data [6]. As can be seen, there is a good agreement between these graphs except in the last moments. This difference can be caused by the effect of heat transfer that occurs when the temperature of the gas inside the capsules drops.

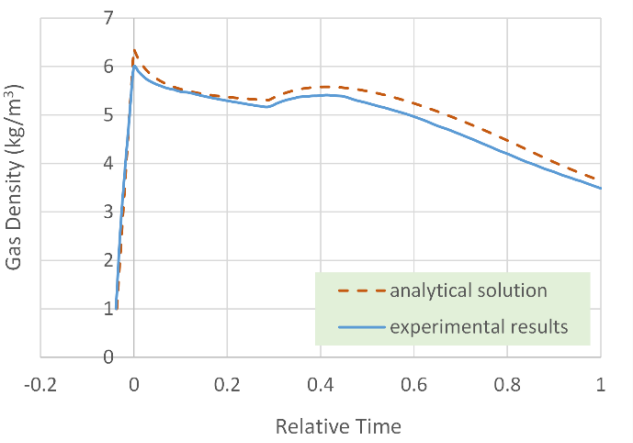

Figure 9. Changes in gas density inside the lower tank using the present model and experimental data.

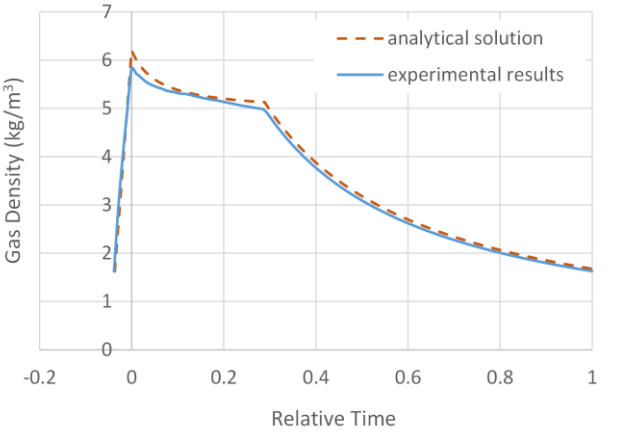

Figure 10. Changes in gas density inside the upper tank using the present model and experimental data.

Table 3. The maximum difference between thermodynamic modeling results and experimental data [6].

Quantity	Tank	Model	Exp. [6]	Error (%)
Mass	Lower	23.26 kg	22.14 kg	5.09
	Upper	5.93 kg	5.76 kg	2.98
	Total	29.06 kg	27.89 kg	4.17
Pressure	Lower	3.82 bar	4.4 bar	13.18
	Upper	1.25 bar	1.86 bar	32.53
Density	Lower	6.2 kg/m^3	5.82 kg/m^3	6.53
	Upper	5.32 kg/m^3	4.95 kg/m^3	7.47

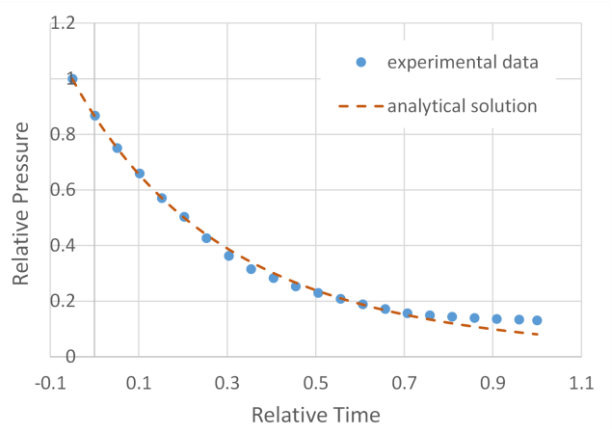

Figure 11. Pressure variations inside the gas-storage capsules using the present model and experimental data [6].

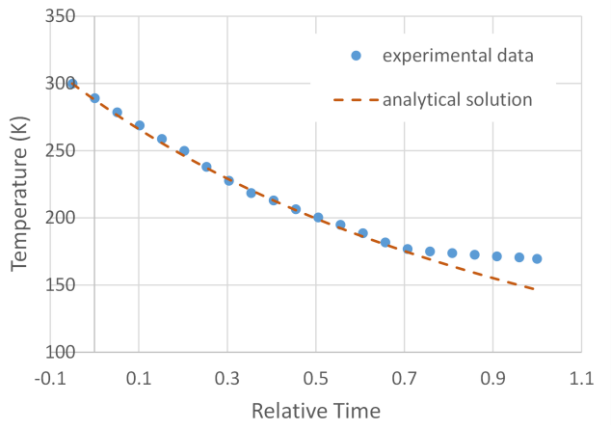

Figure 12. Temperature variations inside the gas storage capsules using the present model and experimental data [6].

Based on the obtained results, the final mass of the gas inside the capsules is about 7.5 kg, which shows the total initial mass of the gas with the amount of mass used for the propellant tanks. Figure 13 shows the time variations of the gas mass inside the capsules for both ideal gas behavior and when the gas compressibility factor, *Z*, is considered. It should be noted that due to the gas pressure loss when passing through the reducing valve and the path until it reaches the tanks, some gas remains inside the capsules. In cases where there is a pressure-reducing valve after the capsules, this valve while reducing the high pressure of the capsules, is responsible for controlling the ullage pressure of the propellant tanks at the nominal value. In the beginning, when the pre-pressurization of the tanks starts and the pressure of the tanks increases, the cross-sectional area of the valve throat decreases until it reaches its minimum value. When the engine starts at time *t=0*, due to the increase in the volume of the ullage on one side and the decrease in the pressure of the gas storage capsules on the other side, the valve increases its cross-sectional area to reach its initial maximum value to prevent the decrease in the pressure of the tanks. From here on, the cross-section of the valve remains constant and the pressure of the propellant tanks gradually decreases due to the decrease in the inlet mass flow rate. Figure 14 shows the changes in the cross-section of the valve's throat.

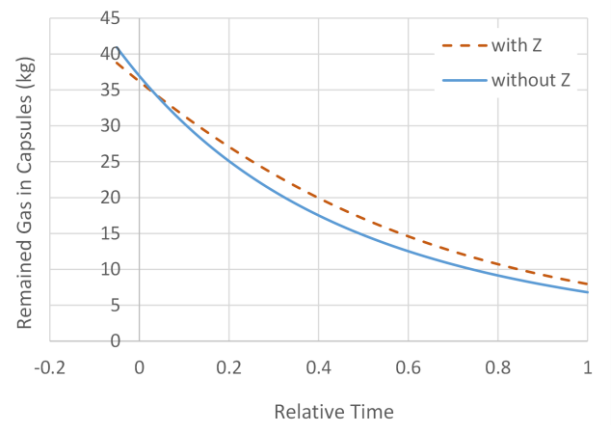

Figure 13. Time variations of gas mass inside the gas storage capsules with and without compressibility factor effect, Z.

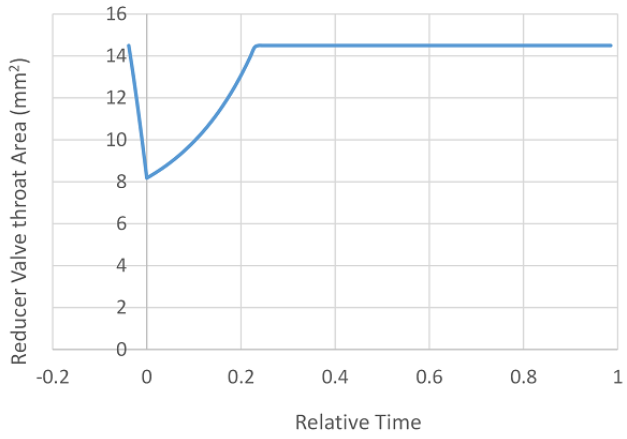

Figure 14. Variations of the cross-sectional area of the valve throat.

5. Conclusions

The objective of this study is to examine the alterations in the properties of the gas within the pressurization system of a liquid fuel rocket by developing an analytical thermodynamic model. The process encompasses the entirety of the engine's operational duration. To validate the performance of the thermodynamic model, the results are compared with the experimental data for the gas properties inside the ullage as well as the gas storage capsules. The following are the most notable outcomes of this study.

- A comparison of the results reveals that the discrepancy in outcomes is most pronounced for the upper tank gas pressure in the last moments, due to ignoring the impact of heat transfer from the wall. This discrepancy reaches approximately 32%. At other times, however, the modeling results predict well the experimental data. In addition, the modeling results show that the mass of the gas used to pressurize the tanks is only about 4% higher than the experimental value.
- For the gas storage capsule, there is also a good agreement between the modeling results and the experimental data except at the end moments due to the

ignoring heat transfer such as propellant tanks. Using the obtained results, it is possible to specify the initial mass of the gas as well as the remained gas in the capsules. In addition, one can observe the approximate changes in the critical cross-sectional area of the pressure-reducing valve, which also acts as an ullage pressure controller.

- As a consequence, the derived model can be employed with an acceptable degree of precision to examine temporal alterations in gas characteristics throughout the course of engine operation. The determination of the system's behavior requires only a few minutes, given the relationships obtained.

Nomenclature

a	acceleration (m/s^2)
C_p	specific heat at constant pressure (J/kg.K)
C_v	specific heat at constant volume (J/kg.K)
g	gravity acceleration (m/s^2)
h	specific enthalpy (J/kg)
H	fluid height (m)
k	gas-specific heat ratio
Ke	kinetic energy (J)
m	mass (kg)
$\dot{m}$	mass flow rate (kg/s)
N	number of capsules
p	pressure (Pa)
Pe	potential energy (J)
$\dot{Q}$	rate of heat transfer (W)
R	gas constant (J/kg.K)
t	time (s)
T	temperature (K)
U	internal energy (J/kg)
$\forall$	volume (m^3)
$\dot{V}$	volume expansion rate (m^3/s)
$\dot{W}$	work per time or power (W)
$\ddot{x}$	acceleration (m/s^2)
z	hight (m)
Z	gas compressibility factor

Greek Symbols

ρ	density (kg/m^3)
ϑ	pith angle (rad)

Subscripts

e	exit
i	inlet
g	gas
l	liquid
0	initial conditions
p	pump
u	ullage

References:

[1] M. Mohseni and M. K. Domfeh, "Numerical analysis of transient vortex formation at the outlet of a tank containing gas-liquid phases," *J. Appl. Fluid Mech.*, vol. 16, no. 11, pp. 2235–2248, 2023, doi: 10.47176/jafm.16.11.1942.

[2] P. Adnani and R. W. Jennings, "Pressurization analysis of cryogenic propulsion systems," in *Proc. 36th AIAA/ASME/SAE/ASEE Joint Propulsion Conf. Exhibit*, 2000, doi: 10.2514/6.2000-3788.

[3] S. In, S. Jeong, and H. Kim, "Investigation on liquid helium pressurization process using a heater in a liquid propellant rocket," *Cryogenics,* vol. 44, no. 6, pp. 467–474, 2004, doi: 10.1016/j.cryogenics.2004.02. 010.

[4] A. Majumdar, J. Valenzuela, A. Leclair, and J. Moder, "Numerical modeling of self-pressurization and pressure control by a thermodynamic vent system in a cryogenic tank," *Cryogenics,* vol. 74, pp. 113-122, 2016, doi: 10.1016/j.cryogenics.2015.12.001.

[5] G. Zilliac and M. Arif Karabeyoglu, "Modeling of propellant tank pressurization," in *Proc 41st AIAA/ASME/ SAE/ASEE Joint Propulsion Conf. and Exhibit*, 2005, doi: 10.2514/6.2005-3549.

[6] H. Karimi, A. Nassirharand, and M. Mohseni, "Modeling and simulation of a class of liquid propellant engine pressurization systems," *Acta Astronaut*, vol. 66, no. 3–4, pp. 539-549, 2010, doi: 10.1016/j.actaastro.2009.07. 018.

[7] M. Gieras and A. Gorgeri, "Numerical modelling of the hybrid rocket engine performance," *Propulsion and Power Res.*, vol. 10, no. 1, pp. 15-22, 2021, doi: 10.1016/ j.jppr.2021.03.001.

[8] L. Wang, Y. Li, C. Li, and Z. Zhao, "CFD investigation of thermal and pressurization performance in LH_2 tank during discharge," *Cryogenics*, vol. 57, pp. 63-73, 2013, doi: 10.1016/j.cryogenics.2013.05.005.

[9] L. Wang, Y. Li, Z. Zhao, and J. Zheng, "Numerical investigation of pressurization performance in cryogenic tank of new-style launch vehicle," *Asia-Pac. J. Chem. Eng.*, vol. 9, no. 1, pp. 63-74, 2014, doi: 10.1002/apj.1797.

[10] Z. Zuo, W. Jiang, X. Qin, and Y. Huang, "A numerical model for liquid–vapor transition in self-pressurized cryogenic containers," *Appl. Therm. Eng.* , vol. 193, 2021, Art. no. 117005, doi: 10.1016/j.applthermaleng.2021. 117005.

[11] S. Ali, N. Abbas, S. A. Khan, I. Malik, and M. Mansha, "Chemical-based hydrogen storage systems: Recent developments, challenges, and prospectives," *Chem. Asian J.*, vol. 19, no. 16, p. e202400320, 2024, doi:10.1002/asia.202400320.

[12] L. Yin, H. Yang, and Y. Ju, "Review on the key technologies and future development of insulation structure for liquid hydrogen storage tanks," *Int. J. Hydrogen Energy*, vol. 57, pp. 1302-1315, 2024, doi: 10.1016/j.ijhydene.2024.01.093.

[13] W. Fan, Y. Ding, and Z. Xiao, "A brand new green coating technology for realizing the regulation of

spherical propellant energy release process," *Def. Technology*, vol. 36, pp. 78-94, 2024, doi: 10.1016/j.dt.2024.02. 008.

[14] L. Wang, Y. Ma, Y. Wang, F. Xie, and Y. Li, "Investigation on pressurization behaviors of two-side-insulated cryogenic tank during discharge," *Int. J. Heat Mass Transf.,* vol. 102, pp. 703-712, 2016, doi: 10.1016/j. ijheatmasstransfer.2016.06. 045.

[15] J. Li, G. Liang, P. Zhu, and X. Wang, "Numerical investigation of the operating process of the liquid hydrogen tank under gaseous hydrogen pressurization," *Aerosp. Sci. Technol.*, vol. 93, 2019, Art. no. 105327, doi: 10.1016/j.ast.2019.105327.

[16] J. Li and G. LIANG, "Simulation of mass and heat transfer in liquid hydrogen tanks during pressurizing," *Chin. J. Aeronaut.*, vol. 32, no. 9, pp. 2068-2084, 2019, doi: 10.1016/j.cja.2019.05.008.

[17] L. Wang, Y. Li, Z. Zhao, and Z. Liu, "Transient thermal and pressurization performance of LO_2 tank during helium pressurization combined with outside aerodynamic heating," *Int. J. Heat Mass Transf.*, vol. 62, no. 1, pp. 263-271, 2013,
doi: 10.1016/j.ijheatmasstransfer.2013.03.021.

[18] Y. Mitikov and O. Shynkarenko, "Reduction of the Pressurization System Final Mass for a Modern Rocket Launcher," *J. Aerosp. Technol. Manage.*, vol. 14, 2022, Art. No. e0122, doi: 10.1590/ jatm.v14.1238.

[19] S. H. Yilmaz, E. Taskesen, K. Roshanaei, and M. Ozkaymak, "Energy Management with Intelligent Plug and Socket," *Gazi Univ. J. Sci.*, vol. 35, no. 3, pp. 969-978, 2022, doi: 10.35378/gujs.933310.

[20] S. Barsi and M. Kassemi, "Numerical and experimental comparisons of the self-pressurization behavior of an LH2 tank in normal gravity," *Cryogenics*, vol. 48, no. 3, pp. 122-129, 2008, doi: 10.1016/j.cryogenics. 2008.01.003.

[21] C. H. Panzarella and M. Kassemi, "Self-pressurization of large spherical cryogenic tanks in space," *J. Spacecr. Rockets*, vol. 42, no. 2, pp. 299-308, 2005, doi: 10.2514/1.4571.

[22] D. A. Fester and P. E. Bingham, "Main Tank Injection (MTI) pressurization of liquid rocket propellant tanks," in *Proc. 54th Int. Astronaut. Congr. Int. Astronaut. Fed. (IAF), Int. Acad. Astronaut., Int. Inst. Space Law*, 2003, doi: 10.2514/6.iac-03-iaa.2.3.06.

[23] L. C. Yang, "Relevant mechanisms affecting the efficiency in detonation of energetic gaseous mixtures," in *Proc. AIAA SciTech Forum Expo.,* 2024, doi: 10.2514/6.2024-2161.

[24] R. Scholl, D. Freudenmann, and S. Schlechtriem, "Microencapsulation of hydrocarbon fuels for monopropellant creation with hydrogen peroxide," *Fuel*, vol. 356, p. 129520, 2024, doi: 10.1016/j.fuel.2023. 129520.

[25] F. W. Childs, T. R. Horowitz, W. Jenisch, and B. Sugarman, "Design guide for pressurization system evaluation liquid propulsion rocket engines," NASA, Tech. Rep. 2334, Nov. 1962.

[26] Y. A. Cengel and M. A. Boles, *Thermodynamics: An Engineering Approach*, 9th ed. New York, NY, USA: McGraw-Hill, 2019.

[27] M. R. Spiegel, S. Lipschutz, and J. Liu, *Schaum's Outline: Mathematical Handbook of Formulas and Tables*, 2nd ed. New York, NY, USA: McGraw-Hill, 1998.

[28] G. F. Pinder, *Numerical Methods for Solving Partial Differential Equations: A Comprehensive Introduction for Scientists and Engineers*, 1st ed. Hoboken, NJ, USA: Wiley, 2018.

[29] A. F. El-Sayed, *Aircraft Propulsion and Gas Turbine Engines*, 2nd ed. New York, NY, USA: CRC Press, 2017, doi:10.1201/9781315156743.

[30] C. Borgnakke and R. E. Sonntag, *Fundamentals of Thermodynamics*, 8th ed. Hoboken, NJ, USA: Wiley, 2013.

[31] Z. Wang, Z. Shao, and H. Chen, "Robust sensor optimization for liquid propellant rocket engine model parameter estimation," *IEEE Trans. Aerosp. Electron. Syst.*, vol. 60, no. 4, pp. 4994–5009, 2024, doi:10.1109/TAES.2024.3384176.